Express Polymer Letters Vol.16, No.11 (2022) 1128–1144
Available online at www.expresspolymlett.com
https://doi.org/10.3144/expresspolymlett.2022.83

express polymer letters

Research article

Luminescent biodegradable polycaprolactone materials prepared by blending with bio-based hyperbranched polymers

Si Qi Huang[1,2], *Wen Hong Ruan*[1,2*], *Ze Pu Wang*[1,2], *Ming Qiu Zhang*[1,2]

[1]Key Laboratory for Polymeric Composite and Functional Materials of Ministry of Education, School of Chemistry, Sun Yat-sen University, 510275 Guangzhou, China
[2]Guangdong Provincial Key Laboratory for High Performance Polymer-based Composites, 510275 Guangzhou, China

Received 13 April 2022; accepted in revised form 2 July 2022

Abstract. It is the pursuit to give biodegradable polycaprolactone (PCL) luminescence properties while maintaining its biocompatibility in a feasible way. For this purpose, bio-based luminescent furan-terminated hyperbranched polymers (HBPFs) have been synthesized, and the degrees of branching (*DB*) of HBPFs are varying from 0.47 to 0.55 as the changing feeding ratio of monomers. All HBPFs exhibit low glass transition temperature (T_g), great fluidity, and bright yellow fluorescence in solution under ultraviolet (UV) light. The ultraviolet/visible (UV/Vis) and fluorescence spectra show that the HBPFs have characteristics of cluster-induced emission (CIE) from the non-conventional chromophores with the concentrations increased. Furthermore, PCL-based materials blending with the HBPFs are also prepared. It is found that the PCL-based blends emit white fluorescence, and the fluorescence intensity is influenced by the contents and *DB* of HBPFs. The morphologies of HBPFs/PCL show that the HBPFs with low contents and high *DB* is well-distributed in PCL, which is conducive to electron transmission and groups-clustering, further enhancing fluorescence emission. The rheological analysis reveals that HBPFs could decrease the viscosity of blends, indicating that HBPFs can play a role as flow modifiers in melt processing. Crystallization behaviors show that the crystallization degree (X_c) of PCL is increased owing to the effects of heterogeneous nucleation of HBPFs (*i.e.* X_c for neat PCL is 60.3% while 5 wt%HBPF-3/PCL is 71.9%). As a result, the modulus of PCL blends is improved. This kind of biocompatible blends with good comprehensive properties and fluorescence characteristics are expected to be applied in the preparation of biomedical materials for *in-situ* non-invasive detection.

Keywords: *biodegradable polymers, polymer blends and alloys, material testing, hyperbranched polymers, fluorescence-emitting blends*

1. Introduction

In recent decades, green biodegradable polymeric materials, including polycaprolactone (PCL) [1], poly(L-lactic acid) (PLLA) [2], poly(glycolic acid) (PGA) [3, 4], and their composites [5–7] have been applied extensively in biomedical materials fields, particularly in the tissue engineer scaffolds. However, the behavior of these biomaterials after implantation cannot be monitored because such materials are unable to respond to *in-situ* non-destructive detection techniques. Bioimaging, such as computed tomography (CT), magnetic resonance imaging (MRI), and optical imaging, has become a crucial approach for non-invasively monitoring [8]. However, MRI is more suitable for determining soft tissues and limited accessibility for hard structures, while long-time CT detection has potential harm to human bodies due to ionizing radiation [9]. The fluorescence imaging technique, as a type of optical imaging, has become one of the most useful ways for

*Corresponding author, e-mail: cesrwh@mail.sysu.edu.cn

in-situ detection because of its high sensitivity, real-time feedback, and cost-effectivity [10].

Because of the ready availability of fluorescence imaging, enhancing the fluorescence response of biomaterials so that they can be detected by fluorescence imaging has become a focus of research. Generally, the purpose of luminescing bio-materials is achieved by the combination of marker molecules [11], inorganic luminescent nanoparticles with matrix [12, 13], or by grafting the luminescent groups in prepolymers [14–16]. However, for physical blending, labeled molecules easily leach from the scaffolds due to their micromolecular structure and weak interaction with the matrix, meanwhile, inorganic luminescent nanoparticles, such as perovskite, are usually too expensive to manufacture on a large-scale. As for the chemical modification, there is always a long and not eco-friendly process from designing the luminescent molecules to anchoring them to the prepolymers. And the mechanical performances of biomaterials modified by the above methods are not comparable to the commercial ones. Therefore, it is important to develop a new 'green' approach to acquiring luminescent biomaterials with biocompatibility and good mechanical performance.

Hyperbranched polymers (HBPs), a class of topological polymers, can be prepared in different generations with readily scalable quantities based on the different feed ratios of core and arms [17]. They are typical three-dimensional architecture and non-entangled for their relatively short chains. Therefore, HBPs exhibit low viscosity, good solubility, compatibility, *etc*. [18–21]. In the previous studies, the HBPs could greatly reduce the viscosity of the polymer matrix, which basically improves the processability while maintaining the thermal stability and mechanical strength compared to low molecular weight flow modifiers [22]. In addition, HBPs that contain carbonyl groups (C=O) and hydroxyl groups (–OH) is a class of bulk luminescent polymers because of the aggregations and electron transitions from C=O and –OH. Thus the HBPs have been utilized in broad photoluminescent applications, such as biosensors [23], fluorescence imaging [24], and drug delivery area [25].

On the other hand, furan and furan-based derivatives are a kind of rigid heterocyclic compounds widely found in natural products, which can be extracted from agricultural wastes such as rice husks and oat husks as well as wood chips, thus they are considered as a class of environmentally friendly bio-based materials [27, 28] with good biological [29] and pharmacological activities [30, 31], including antioxidant [32], antiviral and antibacterial, *etc*. [33]. Considering HBPs possess a large number of end-group, which could react with other functional groups for further modification, the furan group could be easily introduced into HBPs to prepare furan-terminated hyperbranched polymers (HBPFs) with biocompatibility. In this way, the interactions between the bio-based HBFPs and the biopolymer matrix can be enhanced to prevent HBPFs from leaking from the biomatrix and releasing toxicity to human bodies. Therefore, blending the luminous bio-based HBPFs with bio-polymers is expected as an effective way to fabricate the labeled biomaterials. However, the fluorescence characteristics of furan-terminated hyperbranched polymers (HBPFs) and of their blends have not been reported.

Based on the above analysis, cost-effective and fluorescence-emitted furan-terminated hyperbranched polymers (HBPFs) have been synthesized through step-growth polymerization reactions and terminal modifications with a degradable citric acid (CA) as a monomer [26], a bio-based primary amine furfuryl amine (FA) as terminated groups in this paper [27, 28]. Through controlling the feeding ratios of monomers, the as-synthesized HBPFs with different degrees of branching (*DB*) were prepared. The structural and fluorescent characteristics of HBPFs were investigated. Furthermore, considering PCL is the most used biomaterial not only due to its biodegradability and biocompatibility but also the desired mechanical strength, HBPFs/PCL blends have also been prepared. A comprehensive study on the effect of different generations of HBPFs on luminescent properties, rheological, crystallization behaviors, and mechanical properties of PCL composites was also examined. It is anticipated to develop a feasible route by blending with bio-based hyperbranched polymers to acquire potential luminescent biomaterials for *in-situ* non-invasive detection applications.

2. Experimental section

2.1. Materials

Citric acid (CA), p-toluenesulfonic acid (PTSA), 1,2,4-benzeneticarboxylic anhydride (TMA), epichlorohydrin (ECH), furfuryl amine, and sodium hydroxide (NaOH) were purchased from Aladdin Reagent Co., Ltd. (Shanghai, China). Sodium sulphate

(Na_2SO_4) was purchased from General-Reagent (Shanghai, China). Linear thermoplastic polycaprolactone (PCL, M_w = 80 000 g/mol) was purchased from Energy Chemical (Shanghai, China). All of the chemicals were used as received.

2.2. Synthesis of furan-terminated hyperbranched polymers with different generations

Furan-terminated hyperbranched polymers with different generations (HBPF-n, *n* means generation) were synthesized based on three steps. Firstly, various generations of carboxyl-terminated hyperbranched polyesters were prepared by an esterification reaction with various molar ratios of TMA and CA. Then epoxy-terminated hyperbranched polymers were prepared by the reaction of HBPC-n and ECH. Finally, furan-terminated hyperbranched polymers were synthesized by a ring-opening reaction between HBPE-n and furfuryl amine.

2.2.1. Synthesis of carboxyl-terminated hyperbranched polymers (HBPC-n)

HBPC-n (*n* = 1, 2, 3) were synthesized by the esterification reaction between TMA and CA with various molar ratios. The typical process for the synthesis of HBPC-1 with a molar ratio of TMA and CA of 1:3 was followed. 7.68 g (0.04 mol) TMA, 23.05 g (0.12 mol) CA, 0.31 g PTSA, 150 ml 1,4-dioxane, 200 ml toluene were added consecutively to a three-necked round-bottomed flask equipped with a nitrogen inlet, a condenser, and a water trap. The reaction was first carried out at 105 °C for 6 h, then heated to 125 °C for 6 h. A yellow solid was obtained after the solvents were removed under reduced pressure. A similar synthetic process for HBPC-2, and HBPC-3 could be obtained by the molar ratios of TMA and CA of 1:12 and 1:39, respectively.

2.2.2. Synthesis of epoxy-terminated hyperbranched polymers (HBPE-n)

HBPE-n (*n* = 1, 2, 3) were synthesized by a two-step method. The typical process for the synthesis of HBPE-1 was followed. First, 5.86 g (0.008 mol) HBPC-1 and 50 g ECH were added to a three-neck flask equipped with a condenser, a thermometer, and a nitrogen inlet. The mixture was stirred for 3 h at a temperature of 115 °C. The excess ECH was removed under reduced pressure. About 200 ml ethyl acetate was added to dissolve it entirely after the mixture cooled to the ambient temperature. Then 27 g NaOH was introduced, and the reaction was stirred for 5 h at room temperature. After the compound was washed by 75 ml of ultrapure water and the organic phases were combined. The obtained organic layer was washed with 10 ml of ultrapure water three times, then Na_2SO_4 was added to remove water. A yellow, low viscosity transparent liquid with a yield of 46% was obtained after the solvent was removed by rotary evaporation. HBPE-2 and HBPE-3 were synthesized by a similar process with a yield of 43 and 40%, respectively.

2.2.3. Synthesis of furan-terminated hyperbranched polymers (HBPF-n)

HBPF-n (*n* = 1, 2, 3) were synthesized by reacting HBPF-n with furfuryl amine. The typical process for HBPF-1 was followed. Briefly, 0.003 mol HBPE-1 was dissolved in 50 ml DMF in a three-necked round-bottomed flask equipped with a nitrogen inlet, and 0.054 mol furfuryl amine was added into the solution. After the mixture was stirred for 12 h at 50 °C, the excess furfuryl amine and DMF were removed under reduced pressure, and a viscous brownish-black liquid was obtained.

2.3. Preparation of HBPF-n/PCL blends

The HBPF-n/PCL blends were obtained by mechanically mixing HBPF-n (*n* = 1, 2, 3) with PCL using Haake torque rheometer (Potop, RTOI-30/10, Guangzhou, China) at a temperature of 100 °C for 10 min. Before blending, PCL and HBPF-n were dried in a vacuum oven at 40 and 60 °C for 24 h, respectively. Then the polymer blends were compressed into the mold to confer flat or other specific shapes for testing. Three PCL-based different composites were prepared with HBPF-n (*n* = 1, 2, 3) from 5 to 25 wt% and expressed as 5, 15, 25HBPF-n/PCL (*n* =1, 2, 3) in all the figure for simplicity.

2.4. Characterizations

Nuclear magnetic resonance (NMR), ^{1}H NMR spectra were recorded on AVANCE III 400 MHz spectrometer (400 MHz, Bruker, Karlsruhe, Germany) with dimethyl sulfoxide-d_6 (DMSO-d_6) as the solvent.

Fourier transform infrared (FTIR) spectra were performed using a FTIR spectroscopy (Thermo Nicolet Nexus 670, USA) from 400 to 4000 cm^{-1} in transmission mode and attenuated total reflectance (ATR)

mode for the samples of hyperbranched polymers and blends with matrix, respectively. The phased microstructures were characterized by micro-FTIR spectroscopy with imaging microscopy (Thermo Fisher, USA) at room temperature. The absorption spectra were collected on a 200 μm×200 μm square rectangle. For the sample preparation, the mixture was dropped on an aluminum plate, and a thin film was obtained after solvent evaporation. Before micro-FTIR experiment, the common FTIR spectra of samples of PCL, HBPF, and HBPF/PCL were collected to select the marked peak.

Rheological measurements were carried out in oscillatory mode on a rheometer (Kinexus pro+, Malvern Instrument, UK). (a) For the HBPF-n, parallel plate geometry with a diameter of 40 mm and a gap of 1 mm was employed for temperature sweep (25–80 °C) at the strain of 10% and the frequency of 1 Hz. (b) For the HBPF-n/PCL blends, all the samples were hot-compressed to prepare the disc shape with a diameter of 20 mm and a thickness of 1 mm. Parallel plate geometry with a diameter of 20 mm and a gap of 1 mm was employed. Temperature sweeps were carried out from 60 to 150 °C at a heating rate of 2 °C/min under the frequency and strain of 1 Hz and 0.1%, respectively. A dynamic strain sweep was conducted to determine a strain within the linear viscoelastic region (LVER) before all the tests.

The T_g of HBPF-n and the crystallization behavior of the HBPF-n/PCL composites were carried out using differential scanning calorimetry (DSC 4000, PerkinElmer, USA). (a) For T_g of HBPF-n, 3.0–5.0 mg HBPF-n were first heated up to 100 °C and kept at this temperature for 5 min. Then, it was cooled to -60 °C for 3 min at a rate of 10 °C/min. Afterward, a heating scan was taken from –60 to 100 °C. (b) For the HBPF-n/PCL blends, the crystallization behaviors of the samples were performed in the temperature range of –50 to 150 °C at heating rates of 10 °C/min. The second run of these processes was used to analyze the crystallization degree. The weight of the blends was kept between 5.0–6.0 mg and all the tests were performed under N_2 atmosphere at a flow rate of 30 ml/min.

The visualization of HBPF-n/PCL composites crystallization was recorded on polarized optical microscopy (DM2700P, Leica, Germany) equipped with a hot stage (LTS420, Linkam, UK) to investigate the HBPF-n' effects on the PCL crystallization. The samples were sandwiched between two glass slides, heated to 100 °C for 10 min, then rapidly cooled to 40 °C for isothermal crystallization to observe heterogeneous nucleation.

The morphology of the HBPF-n/PCL blends was observed by scanning electron microscopy (SEM) (S-4800, Hitachi, Japan). The surfaces of the blends were sputter-coated with gold before observation.

The luminescence spectra of both HBPF-n and composites were collected with a fluorescence spectrophotometer (F-4600, Hitachi, Japan) equipped with monochromatic Xe lamp as an excitation source. The samples of the composites were compressed with a thickness of 0.5 mm. The slits of both excitation and emission were set at 5 nm, and the scan wavelength speed was 1200 nm/min.

Fluorescence visualization of blends was observed by fluorescence microscopy (Axio Observer, Carl Zeiss, Germany) under UV excitation to obtain fluorescent images. For the sample preparation, the mixture was dropped on a glass slide, and a thin film was obtained after solvent evaporation.

The tensile tests of dumbbell-shaped HBPF-n/PCL composites were done on a universal testing machine (WD-5A, Guangzhou, China) at a speed of 50 mm/min and at room temperature, for each sample was repeated five times.

3. Results and discussion

3.1. Preparation, structure, and properties of HBPF-n (*n* means generation, *n* = 1, 2, 3)

3.1.1. Structural characterization of HBPF-n

The preparation process of HBPFs through step-growth polymerization reactions are shown in Figure 1a. Fourier transform infrared spectroscopy (FTIR) spectra of the first generation of carboxyl-terminated hyperbranched polymer (HBPC-1), epoxy-terminated hyperbranched polymer (HBPE-1), furan-terminated hyperbranched polymer (HBPF-1) are shown in Figure 1b. For the HBPC-1, the peak at 1218 cm^{-1} is attributed to the vibration of C–O–C groups. The strong absorption peak at 1729 cm^{-1} corresponds to the C=O bonds. The wide absorption peak at 3000–3480 cm^{-1} belongs to the vibration of the –OH from –COOH groups. The absorption peaks around 1850 cm^{-1} of anhydride groups from 1, 2, 4-benzeneticarboxylic anhydride (TMA) have not been found, which shows that the anhydride groups have reacted completely. For the HBPE-1, the narrowed absorption peak around 3300 cm^{-1} and the appearance of the absorption peak at 911 and 849 cm^{-1} suggests

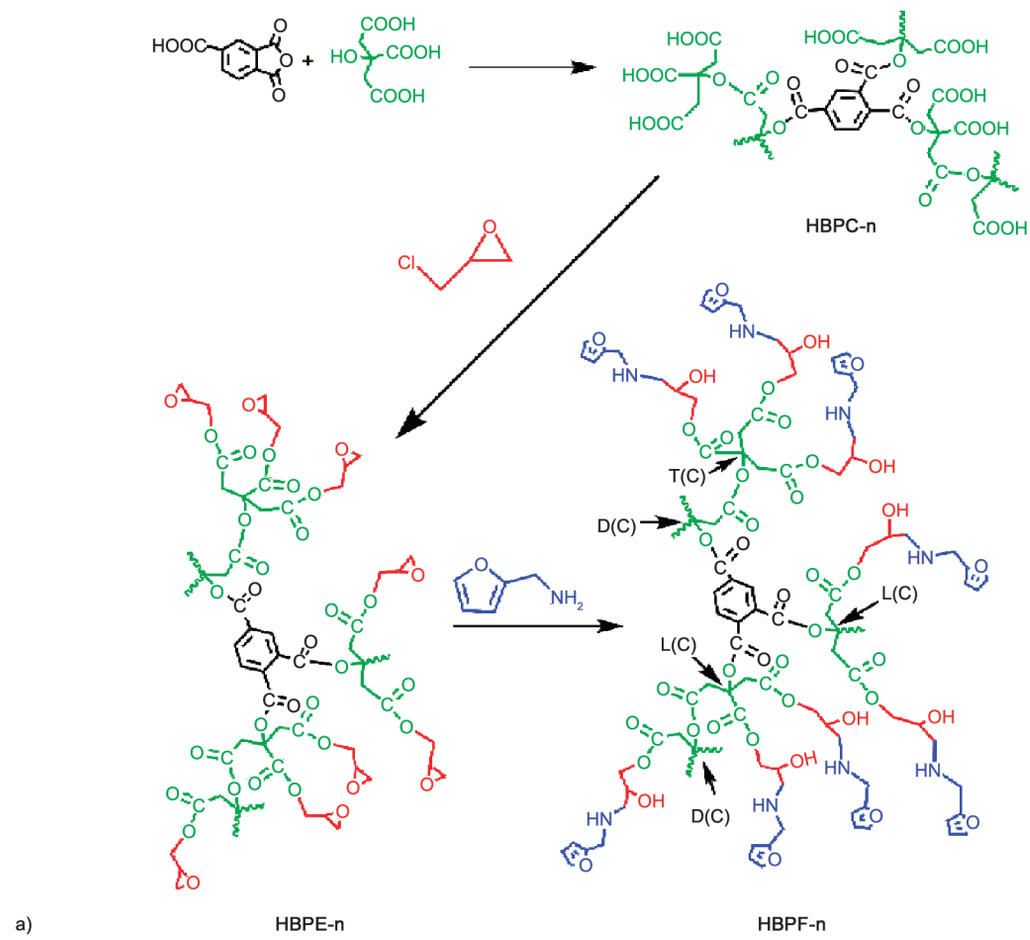

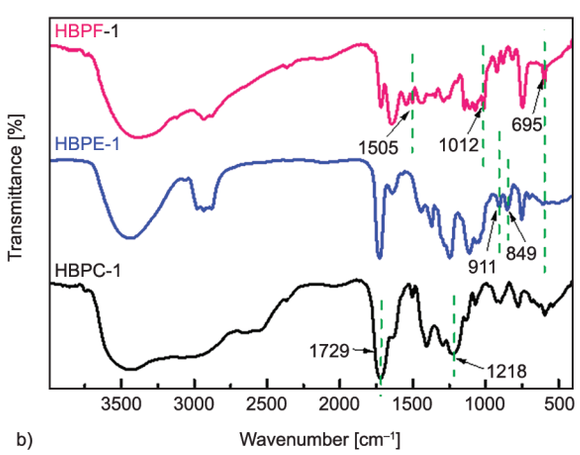

Generation, *n*		Molar ratio of [TMA]/[CA]/[F][a]	Degree of branching, *DB*[b]
	1	1/3/9	0.47
	2	1/12/27	0.50
	3	1/39/81	0.55

[a]Feed molar ratios; 'F' is the abbreviation of furanyl-amine.
[b]The degree of branching (DB) are calculated based on Equation (1).

c)

Figure 1. (a) The synthesized process of HBPF-n; (b) The FTIR spectra of HBPC-1, HBPE-1, HBPF-1; (c) The generation, molar ratios of [TMA]/[CA]/[F] and degree of branching (*DB*) of HBPF-n (*n* = 1, 2, 3).

that the end groups of –COOH of HBPC-1 have reacted and the epoxy groups have generated. For the HBPF-1, the new formation of absorption peaks at 695, 1012, 1505 cm^{-1} are ascribed to the furan heterocycles.

Different generations of HBPFs have similar chemical groups but different topological structures, as shown in Figure 1c. Degree of branching (*DB*) is one of the most useful structural parameters to characterize the topology of HBPs, which can be defined as (Equation (1)):

$$DB = \frac{D+T}{D+T+L} \quad (1)$$

where *D*, *T*, *L* are the dendritic, terminal, and linear units in hyperbranched polymers, respectively, which can be integrated from ^{1}H NMR or ^{13}C NMR spectra [29, 30]. Figure 2a shows the ^{1}H NMR spectra of

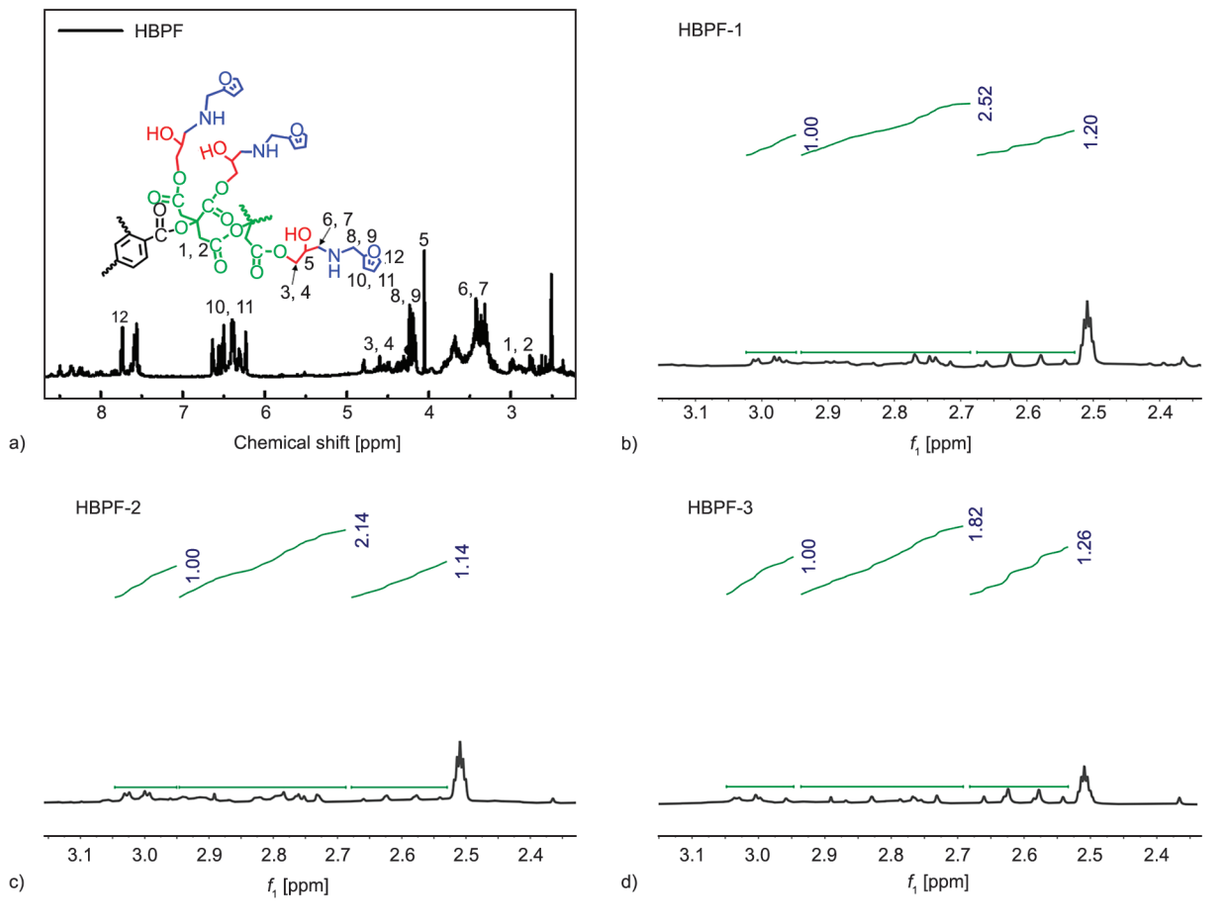

Figure 2. (a) The ^{1}H NMR spectra of HBPF-1; (b–d) the ^{1}H NMR spectra for dendritic, linear and terminal units of HBPF-1, HBPF-2, HBPF-3, respectively.

HBPF. The characteristic peaks of 6.2–6.7 and 7.7 ppm are assigned to the resonance of the protons of furan rings, and the peaks around 2.53–3.05 ppm are the protons of $-CH_2$ from CA, which can be used to calculate the *DB* of HBPFs. The assignments of dendritic, linear, and terminal units of HBPF-n determined by ^{1}H NMR are shown in Figure 2b–2d [31]. The calculated *DB* values based on Equation (1) are 0.47, 0.50, 0.55 for HBPF-1, HBPF-2, HBPF-3, respectively, suggesting that more branching units exist in higher generations of HBPFs, which are coordinated with the higher molar ratios of furfuryl amine/CA/TMA (Figure 1c).

3.1.2. Thermal behaviors and rheological properties of HBPF-n

Hyperbranched polymers usually exhibit low glass transition temperature (T_g) values because of their unique three-dimensional, highly branched topological structure without chain entanglement. The results of differential scanning calorimetry (DSC) measurement show that all the generations of HBPFs are amorphous polymers with T_g of –21.88, –26.60, –23.91 °C for HBPF-1, HBPF-2, HBPF-3, respectively (Figure 3a). The HBPF-2 has the lowest T_g values, indicating that it has well chain-flexibility due to relatively long chains and appropriate intermolecular interaction compared to HBPF-1 composed of short chains, while HBPF-3 is rich in hydrogen bonds, resulting in stronger molecular interactions and higher T_g [32].

Figure 3b shows the function of temperature on melt viscosity of HBPF-n (n = 1, 2, 3). All types of HBPFs exhibit a decrease in viscosity with increasing temperature. It is well-known that the viscosity of most polymers decreases with the increase of temperature because of input heat energy. Generally, the *DB* of hyperbranched polymers has a significant influence on their rheological properties, showing that the viscosity would decrease with increasing the *DB* [33]. However, the viscosity of the HBPF-3 with higher *DB* is higher than that of HBPF-2. This may be attributed to the stronger molecular interactions because more H-bonds exist in HBPF-3 structure, causing a higher shear viscosity at low temperatures.

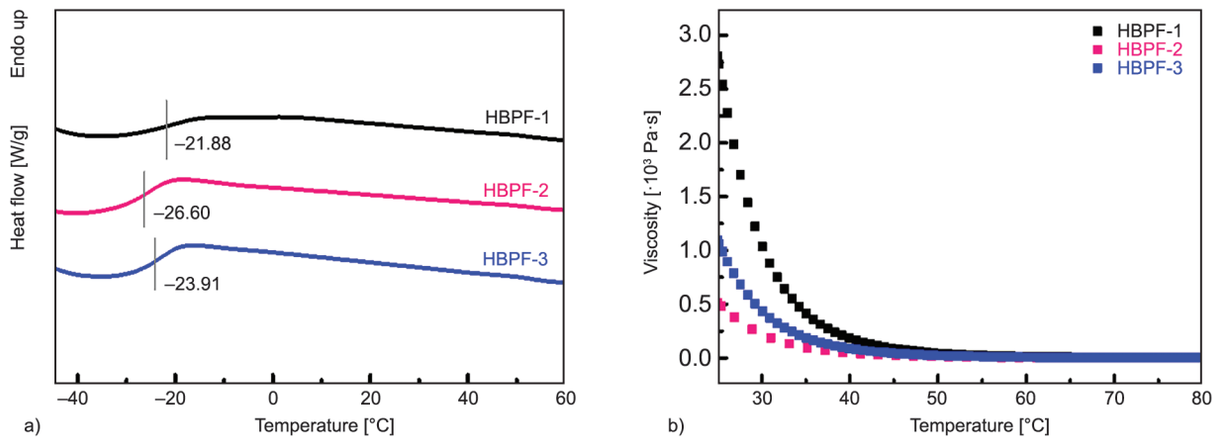

Figure 3. (a) DSC curves of HBPF-n; (b) dependence of HBPF-n viscosity on temperature.

3.1.3. Fluorescent behaviors of HBPF-n

HBPFs contain multiple ester groups, secondary amine, hydroxyl, and furan groups, which are considered the source of non-traditional intrinsic luminescence due to the electronic transitions and the aggregation of these groups. The UV-vis absorption of HBPF-n in solutions is measured (Figure 4a). It is found that HBPFs with different generations have similar UV-vis absorption peaks at around 255 and 295 nm, showing the absorption intensity is decreasing with an increase of *DB* at the same concentration. The peak at 255 nm is associated with π-π* and *n*-σ*

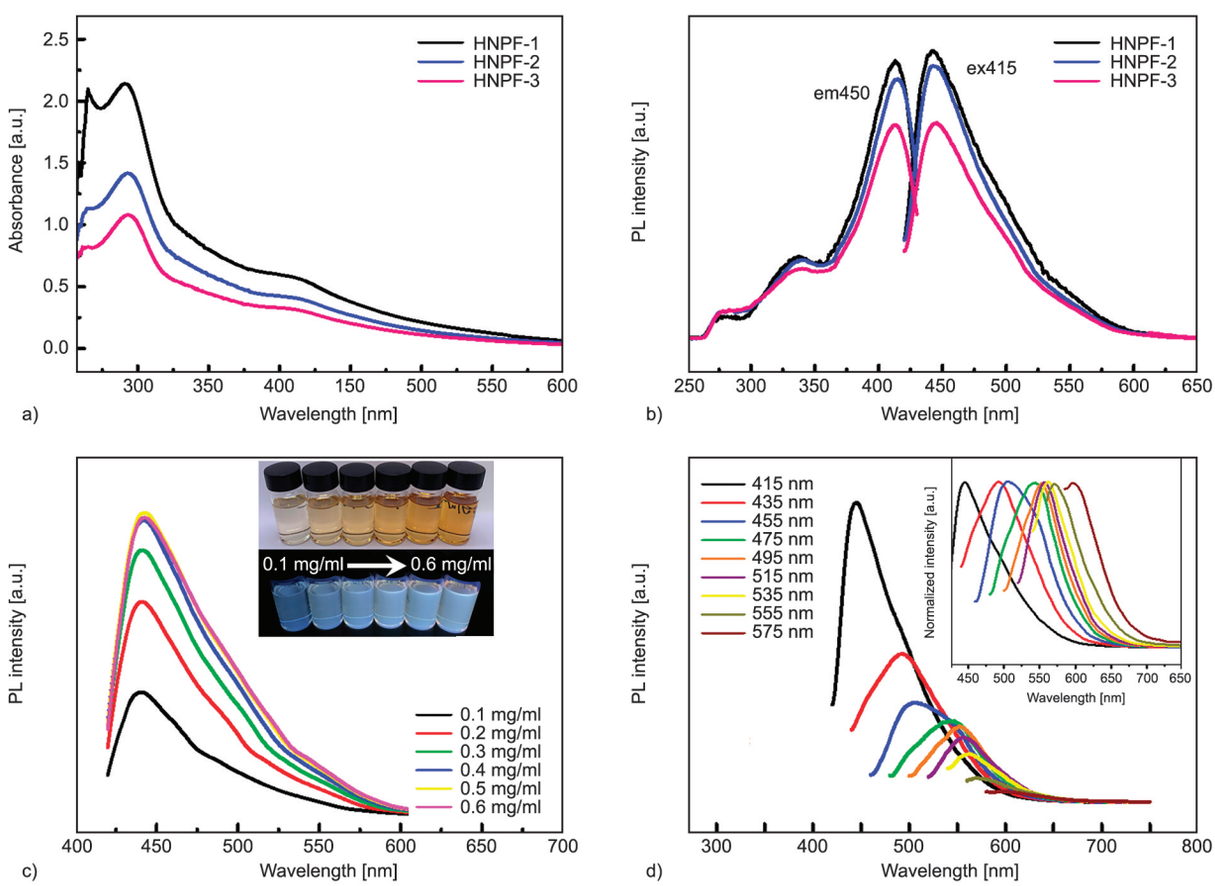

Figure 4. (a) UV-vis spectra and (b) fluorescence spectra of HBPF-n in DMF solution with the same concentration of 0.5 mg/ml. (c) Fluorescence spectra of HBPF-1 in DMF solution with varying concentrations (λ_{ex} = 415 nm) (inset: fluorescence images of HBPF-1 in DMF solution at different concentrations in daylight (top) and 365 nm UV light (below)). (d) Fluorescence spectra of HBPF-1 in DMF solution with the concentration of 1.0 mg/ml excited with varying UV wavelength (inset: normalized fluorescence intensity).

electron transitions from furan rings, C=O and –OH. The peak at around 295 nm is attributed to the n-π^* electron transition of the C=O and –NH– groups (Figure 4a) [21]. Furthermore, the photoluminescence behavior of HBPF-n is measured in Figure 4b. It is noteworthy that the fluorescence spectra of HBPF-n exhibit the same emission behaviors, suggesting that these three hyperbranched polymers have analogous emission mechanisms. The fluorescence intensity of HBPF-n is decreasing with the *DB* increased at the same concentration of 0.5 mg/ml, which is consistent with the results of UV-Vis absorption spectra. This could be attributed to the π-π stacking interactions of the peripheral furan groups, that increasing efficient conjugated length easily generates excimers by more π-π stacking, resulting in luminescence decreasing [34]. The photoluminescence properties of HBPF-1 dissolved in *N*,*N*-dimethylformamide (DMF) with varying concentrations are also investigated. Figure 4c shows that the HBPF-1 exhibit apparent fluorescence intensity enhancing with the concentrations increased looks transparent under daylight, and emits brighter fluorescence under 365 nm UV light irradiation (Figure 4c inset), suggesting a typical cluster-inducing emission (CIE) property [35]. Moreover, to investigate the excitation-dependent emission (EDE) behavior, the emission behavior of HBPF-1 dissolved in DMF is carried out under different UV exciting wavelengths. The emission peaks present a gradual red-shift as the excitation wavelength varies from 415 to 575 nm while the emission intensity begins to decrease (Figure 4d), which is consistent with the results reported in the previous research [20, 21, 36].

3.2. Morphology and properties of HBPF-n/PCL blends

3.2.1. Luminescence behaviors of HBPF-n/PCL blends

The fluorescence emission spectra of PCL films blended with different contents of HBPF-n (n =1, 2, 3) from 0 to 25 wt% are shown in Figure 5. It is worthy to note that the fluorescence intensity of blends excited at 365 nm relates to the *DB* (According to the above results, different *DB* and different generations can be used in the same way for describing HBPFs.) and the contents of HBPF-n. Specifically, the films are prone to exhibit higher fluorescence intensity with the increase of *DB* at the same content of 5 wt%, as HBPF-3 shown in Figure 5a. However, when the content is up to 25 wt%, the fluorescence intensity of blends tends to decrease (Figure 5b). It is found that a small amount of HBPFs imparts higher fluorescence luminescence to PCL than the high loading of HBPFs. Furthermore, pure PCL film has shown weak blue fluorescence emission under the excitation of 365 nm UV light (Figure 5c). This phenomenon may be attributed to the clustering behaviors of C=O from the main linear chains of PCL, according to previous research [37, 38]. On the other hand, HBPF-n/PCL blends exhibit fluorescence emission as that of HBPFs even at a low loading of 5 wt% HBPFs (Figure 5c), which might originate from the electron transition and aggregation of ester, –C=O, –OH, –NH- and furan groups. It is inferred that the content-dependent and *DB*-dependent fluorescence intensity of HBPFs/PCL may be correlated with the influence of interaction between HBPFs and PCL on the morphology of blends.

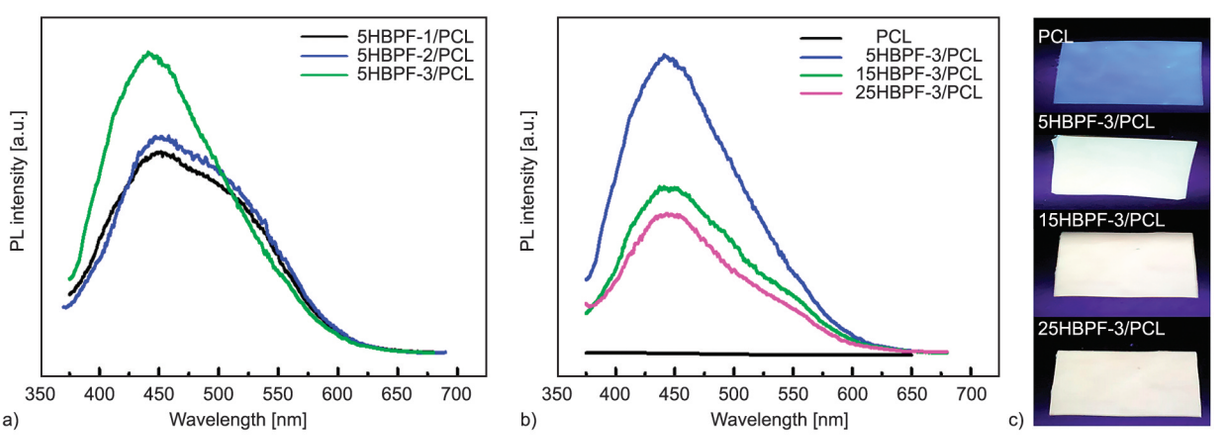

Figure 5. (a) Fluorescence spectra of HBPF-n/PCL (n = 1, 2, 3) films with the same contents of 5 wt%; (b) fluorescence spectra of HBPF-3/PCL with the HBPF contents of 5, 15, 25 wt%; (c) the photo of HBPF-3/PCL films with varying compositions excited at UV light. (Thickness of the films: 0.5 mm, λ_{ex} = 365 nm.)

3.2.2. Morphology of HBPF-n/PCL blends

In order to investigate the luminescence mechanism of HBPFs/PCL, fluorescence microscopy observation is conducted (Figure 6) to study the morphology of blends [39, 40]. It is shown that all the films can emit fluorescence under UV excitation, which coordinates with the results of fluorescence spectra. Specifically, the films with 5 wt% HBPF-n show no significant black agglomerated areas in fluorescent images while presenting more evenly bright domains with the increase of *DB* (comparing Figure 6a with Figure 6b). On the other hand, both fluorescent images of PCL blends with 25 wt% HBPF-1 and HBPF-3 present the dark agglomerated regions distributed in the continuous-bright matrix domain (Figure 6c and 6d). Moreover, it is found that the films blended with HBPF-3 appear to have more significant phase separation phenomena (comparing Figure 6c with Figure 6d) [41]. For the HBPF-n content of 5 wt%, there are more –OH, C=O, and –NH– existing in HBPF-3 with higher *DB*. Figure 7 shows the FTIR spectra of PCL and its blends with HBPF-n (n =1, 2, 3) at the same content of 5 wt%. For the blends, two new peaks of 1652 and 1544 cm^{-1} are seen and assigned to the C=O and –NH– groups from HBPFs, while the –OH absorption region of 3500–3100 cm^{-1} is increased gradually with the increase of *DB* for HBPF-n, thus possessing highly branching structure would improve the probability of electron transition and aggregation of C=O from both HBPF and PCL; moreover, HBPF-3 generate more H-bonds which can play a role of rigidifying the molecular chains which will greatly decrease the non-radiative activation and facilitate the fluorescence emission. As for the HBPF-n contents up to 25 wt%, the generated agglomerated HBPFs would transfer the energy and further quench fluorescence due to the interaction with excited molecules under the UV excitation [42, 43]. On the other hand, more π-π stacking existing in HBPF-3 would further decrease the fluorescence intensity, according to the previous research [44]. Therefore, as for the fluorescence intensity of

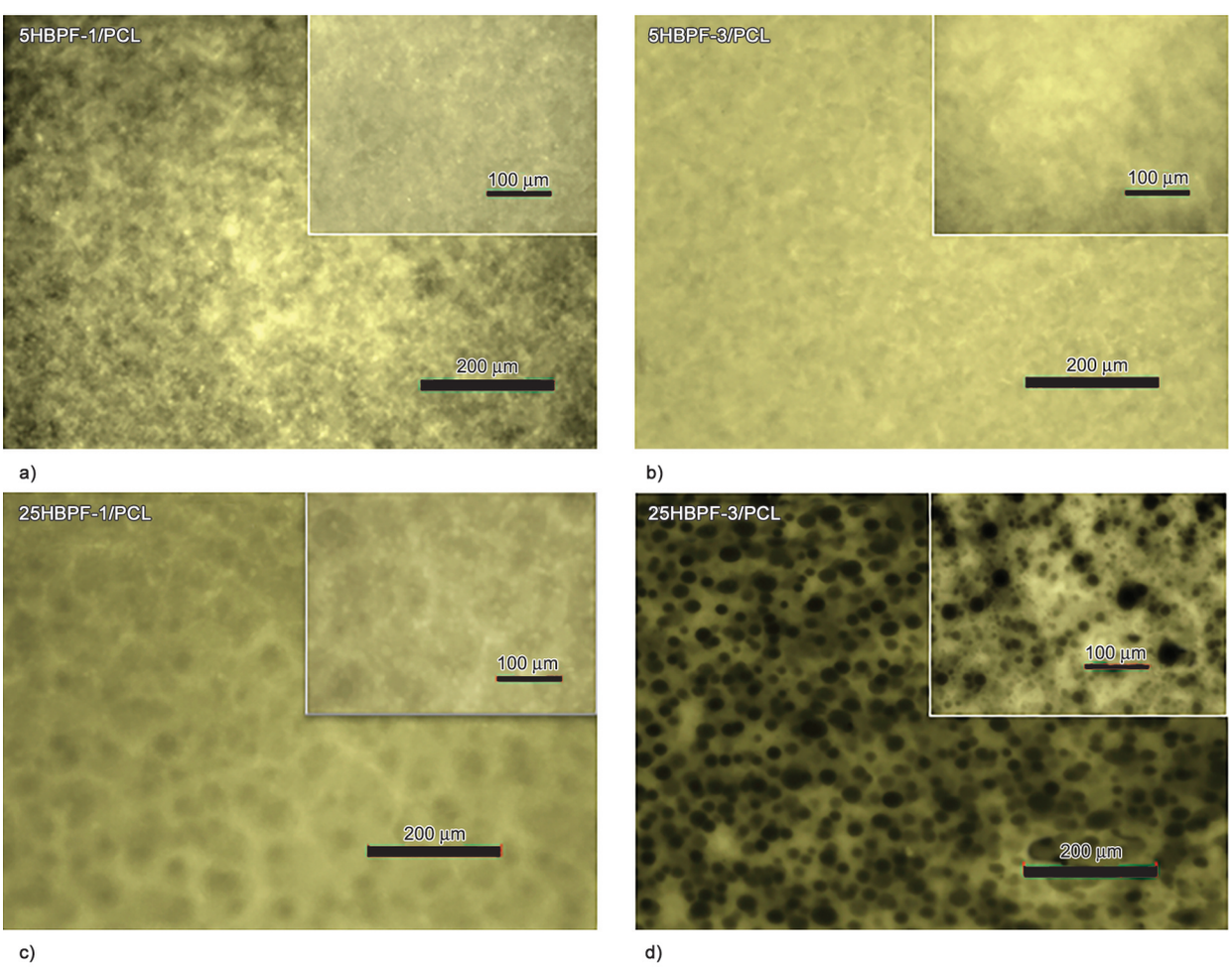

Figure 6. Fluorescence images of PCL blended with HBPF-1, HBPF-3 with the contents of 5 wt% (a and b) and 25 wt% (c and d) under UV light excited.

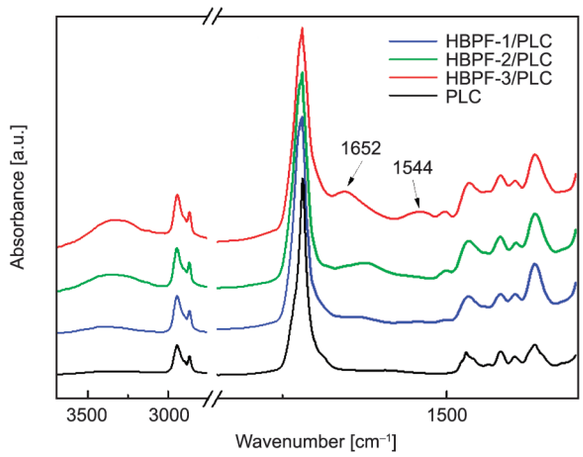

Figure 7. FTIR spectra of PCL and its blends with HBPF-n at the same content of 5 wt% (n = 1, 2, 3).

blends with HBPF-3, there has been a decreasing the tendency with an increase of contents as shown in Figure 5b.

To further confirm the content and *DB* effects of HBPFs on the morphology of blends, the blends are also observed through polarizing microscopy (POM) (Figure 8) and scanning electron microscopy (SEM) (Figure 9). Both Figure 8a and 8b and Figure 9a and 9b show that with the low content of 5 wt% HBPF-n, blends show a homogeneous appearance, indicating HBPF-n is well dispersed in the PCL matrix. The agglomerated HBPF-n phases can be seen by increasing the contents of HBPF-n up to 25 wt% while the phase separation is more pronounced in blends of HBPF-3 with high *DB* (comparing Figure 8c with Figure 8d and Figure 9c with 9d). The micro-FTIR images also confirm the morphology that blends with 25 wt% HBPF-3 have a more obvious microphase separation than that with 25 wt% HBPF-1 (Figure 8e and 8f), which is consistent with the results of fluorescence microscopy as mentioned above

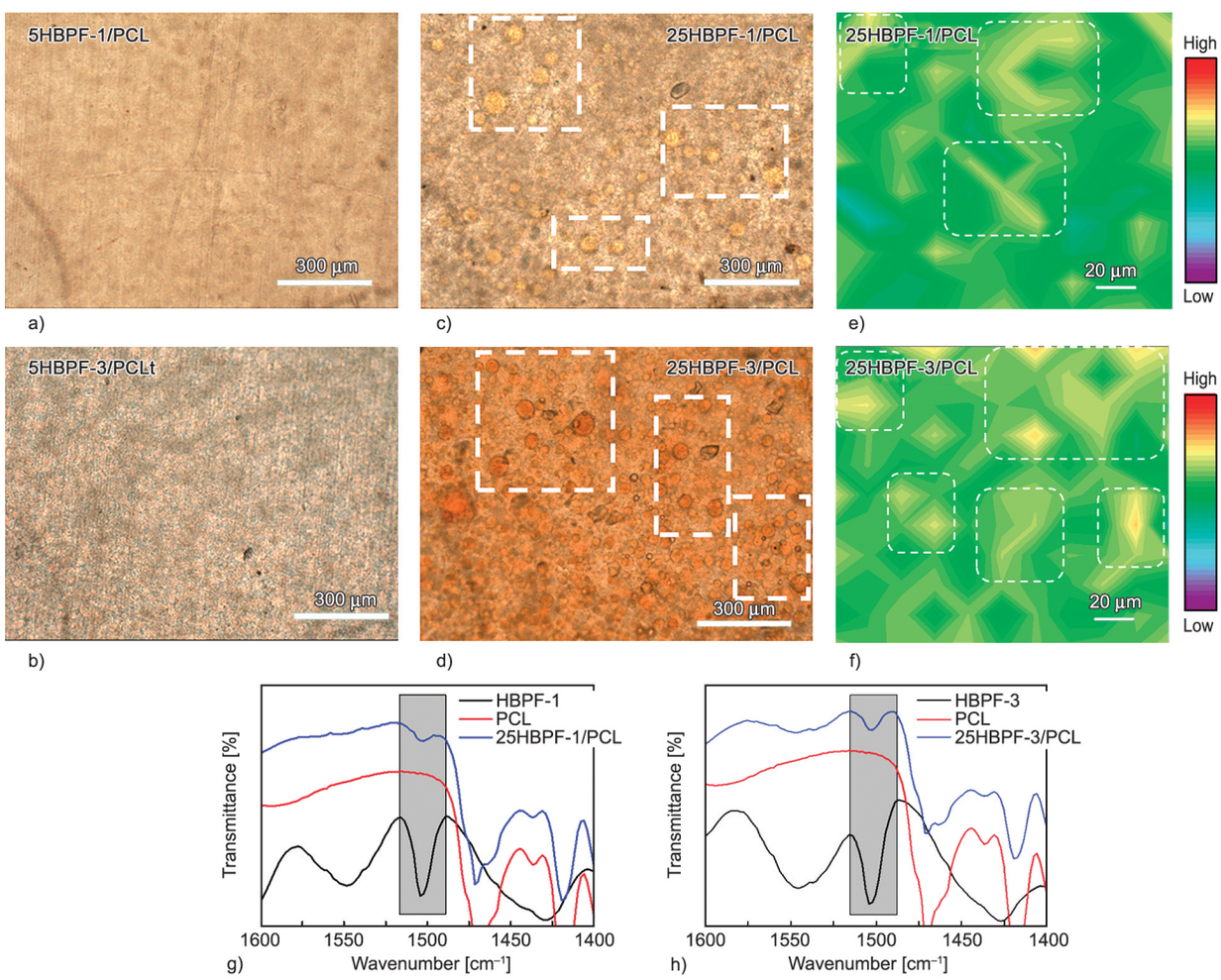

Figure 8. POM images of PCL blended with HBPF-1, HBPF-3 with the contents of 5 wt% (a and b) and 25 wt% (c and d). Micro-FTIR spectroscopy of PCL blended with HBPF-1 (e) and HBPF-3 (f) with the content of 25 wt%. Comparison of FTIR spectra of HBPF-n, PCL, and 25 wt% HBPF-n/PCL, n = 1 (g), n = 3 (h). The gray boxes are the characteristic peak for furan groups that is on the spectra of HBPF-n and is absent in PCL, thus this peak can serve as the marker for micro-FTIR analysis.

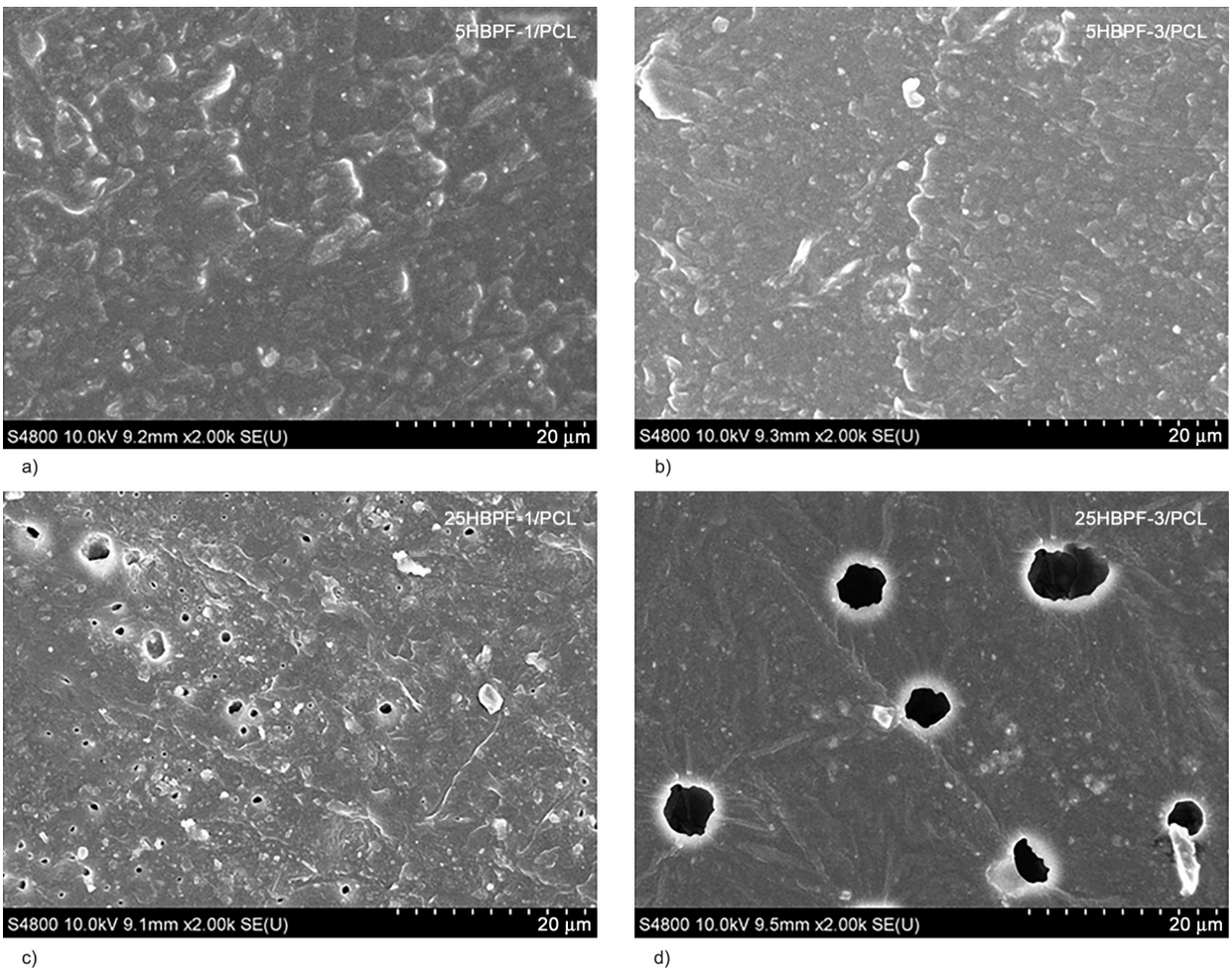

Figure 9. SEM images of PCL blended with HBPF-1, HBPF-3 with the contents of 5 wt% (a and b) and 25 wt% (c and d).

and can be ascribed to stronger molecular interaction of HBPFs. More H-bonds and π-π stacking exist in high contents HBPFs with higher *DB* leading to easily agglomerating in the blends, further increasing the phase separation and decreasing the fluorescence intensity.

3.2.3. Rheological properties of HBPF-n/PCL blends

Aiming to further explore the effects of content and *DB* of HBPFs on the interaction between HBPF-n and PCL, rheological measurements were carried out. As shown in Figure 10, the viscosity, the storage modulus (G'), and loss modulus (G'') of neat PCL and all the blends decrease with increasing temperature and show viscous behavior at the test temperature. After the incorporation of HBPFs, the melt viscosity of PCL decreases further owing to the special topological structure of hyperbranched polymers with multiple end-groups providing more free volume for chain movement, which is typically considered as a type of flow modifier [20]. It is worth noting that the flowability of blends with higher *DB* HBPF-n tends to get better (Figure 10a and 10b). Higher *DB* HBPF-n with more branching chains of lateral groups (–OH) and end-groups (Furan) could disentangle and penetrate into the long linear chains of PCL, thus improving the flowability of the blends and enhancing the interaction between matrix and HBPFs. However, as for the content of HBPFs up to 25 wt%, the viscosity, G' and G'' of the blends markedly reduce, meaning that the internal friction is decreased drastically as adding excessive flow modifier (Figure 10c and 10d), which cannot be dispersed evenly in the matrix. It is further confirmed that the low content of HBPFs can interpenetrate with PCL and facilitate the electron transition, resulting in high fluorescence emission.

3.2.4. Crystallization behavior of HBPF-n/PCL blends

For the blends composed of amorphous hyperbranched polymers of HBPFs and semi-crystalline polymers of PCL, it is needed to investigate the crystallization

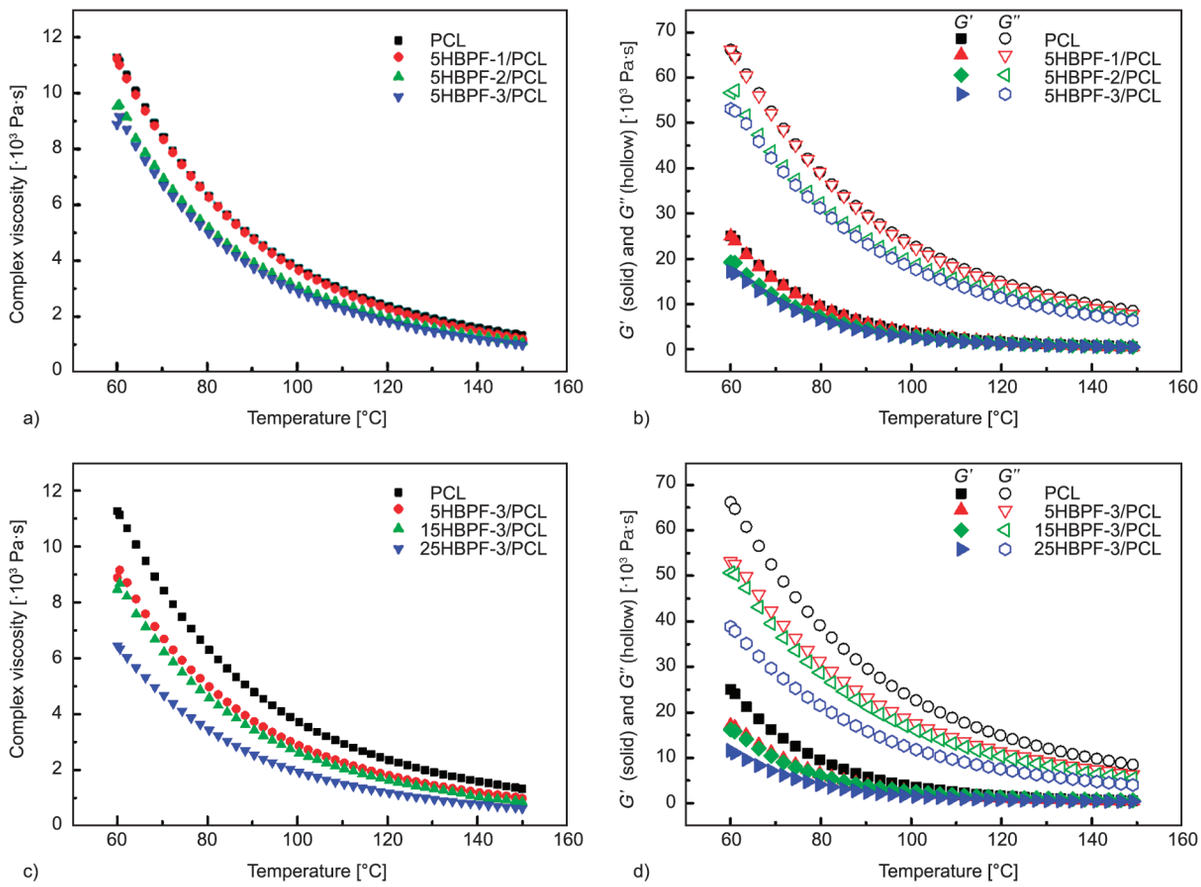

Figure 10. Dependence of PCL and PCL/HBPF-n blends complex viscosity, storage modulus (*G′*), and loss modulus (*G″*) on temperature. (a) and (b) blends with different *DB* at the same content of 5 wt%. (c) and (d) blends with HBPF-3 of different contents (from 0 to 25 wt%).

behaviors which can substantially affect the properties of blends. The results of DSC measurements of HBPFs/PCL with different contents and *DB* of HBPFs are listed in Table 1.

From Table 1, it can be seen that the degree of crystallinity (X_c) of PCL increases with the *DB* increased at low content of HBPF-n. Moreover, for the blends with the increased contents of HBPF-3, the X_c tend to decrease gradually. Figure 11 confirms that 5 wt% HBPF-3/PCL has a higher crystallization density at a shorter time compared to 5 wt% HBPF-1/PCL, and both are faster than PCL as shown in the process of isothermal crystallization. It is demonstrated that low contents and well-distributed HBPFs have heterogeneous nucleation effects on PCL, and HBPFs with higher *DB* could provide more crystalline nucleation sites, resulting in a higher value of X_c. The blends with 25 wt% HBPF-3 have the lowest X_c, and it is confirmed the agglomeration of amorphous phases of HBPFs from the other side would

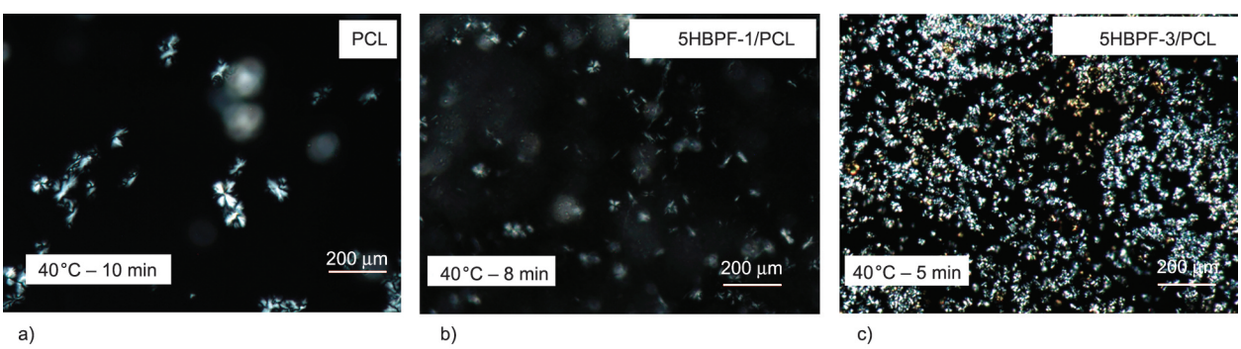

Figure 11. Isothermal crystallization process of PCL (a), 5 wt% HBPF-1/PCL (b), and 5 wt% HBPF-3/PCL (c) at the early stage.

Table 1. Crystallization and melting characteristics of HBPF-n/PCL blends.

Component	T_m[a] [°C]	ΔH_m[b] [J/g]	X_c[c] [%]
Pure PCL	56.18	82.01	60.3
5 wt% HBPF-1/PCL	55.62	82.98	61.0
5 wt% HBPF-2/PCL	55.42	87.87	64.6
5 wt% HBPF-3/PCL	56.44	97.77	71.9
15 wt% HBPF-3/PCL	55.11	84.93	62.4
25 wt% HBPF-3/PCL	55.12	80.33	59.1

[a]T_m denotes the melting temperature of samples in the second run; [b]ΔH_m represents the fusion enthalpy of samples in the second run; [c]The degree of crystallinity (X_c) of the crystalline component can be calculated based on the following equation: $X_c = \Delta H_m/\Delta H_m^0$, where ΔH_m denotes the melting endothermal peaks of samples, and ΔH_m^0 is the melting enthalpy of the 100% crystalline PCL (136 J/g) [45].

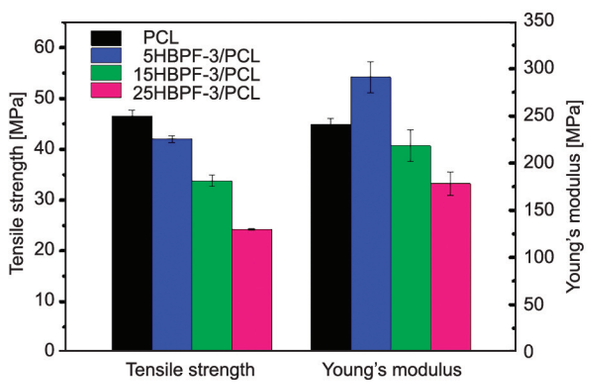

Figure 12. The mechanical properties of the blends with 0, 5, 15, 25 wt% HBPF-3.

restrict the regular arrangement of PCL chains under the crystallization process [41]. Furthermore, the higher X_c would further contribute to preparing robust HBPFs/PCL materials with considerable mechanical strength (Figure 12).

According to previous research, the luminescence behaviors of blends can be affected by the matrix's amorphous or crystalline state [46]. When the matrix is in the crystalline state, the intramolecular motions, such as vibrations and rotations, of luminescent molecules would be strongly restricted, resulting in less non-radiative energy decay but more fluorescence emission, which is a pathway of radiative energy decay for excited molecules. Therefore, fluorescence microscopy can be used to *in-situ* investigate the relationship between fluorescence and crystallization behavior. Figure 13 shows that the fluorescent regions of 5 wt% HBPF-1/PCL increase with time, which is consistent with the change in the crystalline region.

3.3. Discussion on luminescence mechanism of HBPFs/PCL

Based on the above analysis, a schematic drawing to illustrate the effects of contents and *DB* of HBPFs on the morphology and luminescence properties of blends is given in Figure 14. At the low contents, HBPFs is well-distributed in the PCL, and the branching short chain of hyperbranched polymer could be fully extended (Figure 14a), thus the interactions between HBPFs and PCL are conducive to the formation of the electron transmission network and luminescent aggregated 'clusters', further enhancing the fluorescence emission of blends under UV excitation (Figure 6a and 6b). With an increase of *DB* at low content, more heterogeneous nucleation and interactions exist in HBPF-3 and PCL, which would play a role in restricting non-radiative activation and facilitating fluorescence emission (Figure 6b). Meanwhile, more free volume and branching points brought by HBPF-3 are prone to disentangle linear PCL (Figure 14a), leading to an increase in rheological and crystalline properties compared to low *DB*. At the high contents, HBPFs tend to agglomerate in the PCL, owning to strong hydroxyl-hydroxyl bonds and π-π stacking, resulting in microphase separation (Figure 14b, Figure 8c–8f, Figure 9c and 9d), which would lead to energy transfer and dissipation for excited molecules, in addition, more π-π stacking would also decrease the fluorescence emission (Figure 6c and 6d).

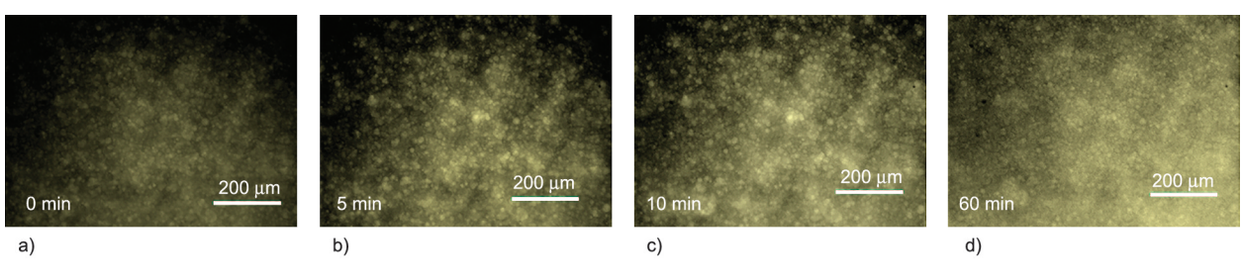

Figure 13. Fluorescence images of *in-situ* observing the change of luminescence area of 5 wt% HBPF-1/PCL under crystallization at room temperature. a) 0 min; b) 5 min; c) 10 min; d) 60 min.

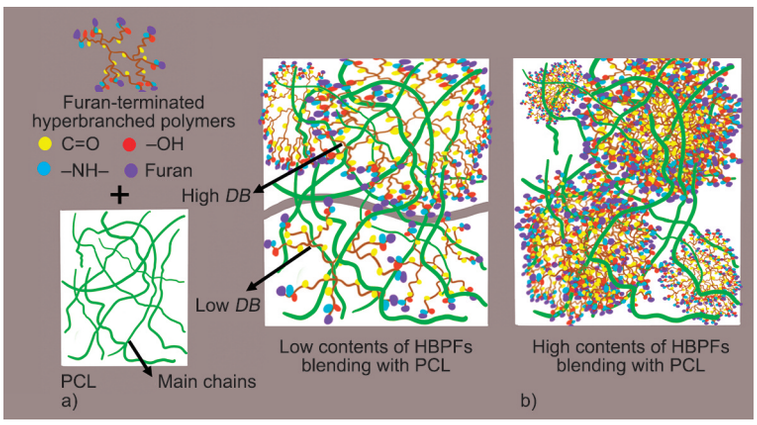

Figure 14. Schematic drawing of effects of HBPFs contents and *DB* on the morphology and luminescence properties of the blends.

4. Conclusions

In conclusion, bio-based furan-terminated hyperbranched polymers (HBPFs) containing C=O, –OH and –NH– groups have been firstly synthesized through green polymerization mostly based on biomass materials including citric acid (CA) and furfuryl amine (FA) and the degrees of branching (*DB*) increase with the increase of generations of HBPF-n (n = 1, 2, 3). All resultant HBPFs exhibit strong yellow fluorescence in solutions under 365 nm UV light and low T_g with better fluidity. The effects of concentration and *DB* of HBPFs on its luminescence intensity are also investigated, showing that the fluorescence intensity of HBPFs solution is increasing with the increase of concentrations, indicating a CIE phenomenon. Meanwhile, with the *DB* increased, the fluorescence intensity of HBPFs tends to decrease owing to the π-π stacking from furan groups.

The HBPFs/PCL bio-blends are prepared by common melt mixing. It is found that the films of blends emit bright white fluorescence in the solid-state, and the fluorescence intensity of blends tends to have a close relationship with the contents and *DB* of HBPFs. Fluorescence microscopy is used to study the luminescence behavior and morphology of the blends, showing that low content HBPFs with higher *DB* would enhance the luminescence of PCL because of the better compatibility and enhanced interface interaction from entanglement between more branching chains and matrix chains, as well as the hydrogen bonds caused by –OH and –NH– on HBPFs. While the high content of HBPFs would inhibit the fluorescence emission of the blends owing to π-π stacking caused by the agglomeration of HBPFs in PCL matrix, which is also observed by POM and micro-FTIR spectroscopy. Studies on rheological and crystalline behaviors also show that the addition of low content of HBPFs would decrease the melt viscosity of PCL and improve the degree of crystalline, indicating HBPFs can be a flow modifier in the processing of PCL-based materials while maintaining the mechanical properties of PCL materials. The method of blending bio-polymers with the appropriate amount of bio-based hyperbranched polymers through conventional melting processing to endow bio-based materials with fluorescence properties is simple and environmentally friendly.

Acknowledgements

The authors thank the support from the National Natural Science Foundation of China (Grants: 52033011 and 52173092), and the Science and Technology Program of Guangzhou, China (202007020001).

References

[1] Backes E. H., Harb S. V., Beatrice C. A. G., Shimomura K. M. B., Passador F. R., Costa L. C., Pessan L. A.: Polycaprolactone usage in additive manufacturing strategies for tissue engineering applications: A review. Journal of Biomedical Materials Research Part B: Applied Biomaterials, 110, 1479–1503 (2021). https://doi.org/10.1002/jbm.b.34997

[2] Raghavendran H. R. B., Natarajan E., Mohan S., Krishnamurithy G., Murali M. R., Parasuraman S., Singh S., Kamarul T.: The functionalization of the electrospun PLLA fibrous scaffolds reduces the hydrogen peroxide induced cytokines secretion *in vitro.* Materials Today Communications, **26**, 101812 (2021). https://doi.org/10.1016/j.mtcomm.2020.101812

[3] Shu X., Liao J., Wang L., Shi Q., Xie X.: Osteogenic, angiogenic, and antibacterial bioactive nano-hydroxyapatite *co*-synthesized using γ-polyglutamic acid and copper. ACS Biomaterials Science and Engineering, **6**, 1920–1930 (2020). https://doi.org/10.1021/acsbiomaterials.0c00096

[4] Castro F., Pinto M. L., Pereira C. L., Serre K., Barbosa M. A., Vermaelen K., Gärtner F., Gonçalves R. M., de Wever O., Oliveira M. J.: Chitosan/γ-PGA nanoparticles-based immunotherapy as adjuvant to radiotherapy in breast cancer. Biomaterials, **257**, 120218 (2020). https://doi.org/10.1016/j.biomaterials.2020.120218

[5] Peng Z., Wang C., Liu C., Xu H., Wang Y., Liu Y., Hu Y., Li J., Jin Y., Jiang C., Liu L., Guo J., Zhu L.: 3D printed polycaprolactone/beta-tricalcium phosphate/ magnesium peroxide oxygen releasing scaffold enhances osteogenesis and implanted BMSCs survival in repairing the large bone defect. Journal of Materials Chemistry B, **9**, 5698–5710 (2021). https://doi.org/10.1039/D1TB00178G

[6] Xu Z., Xu Y., Basuthakur P., Patra C. R., Ramakrishna S., Liu Y., Thomas V., Nanda H. S.: Fibro-porous PLLA/ gelatin composite membrane doped with cerium oxide nanoparticles as bioactive scaffolds for future angiogenesis. Journal of Materials Chemistry B, **8**, 9110–9120 (2020). https://doi.org/10.1039/D0TB01715A

[7] Abdal-hay A., Raveendran N. T., Fournier B., Ivanovski S.: Fabrication of biocompatible and bioabsorbable polycaprolactone/ magnesium hydroxide 3D printed scaffolds: Degradation and *in vitro* osteoblasts interactions. Composites Part B: Engineering, **197**, 108158 (2020). https://doi.org/10.1016/j.compositesb.2020.108158

[8] Cengiz I. F., Oliveira J. M., Reis R. L.: Micro-CT – A digital 3D microstructural voyage into scaffolds: A systematic review of the reported methods and results. Biomaterials Research, **22**, 26 (2018). https://doi.org/10.1186/s40824-018-0136-8

[9] Zhang Y. S., Yao J.: Imaging biomaterial-tissue interactions. Trends in Biotechnology, **36**, 403–414 (2018). https://doi.org/10.1016/j.tibtech.2017.09.004

[10] Jing L., Sun M., Xu P., Yao K., Yang J., Wang X., Liu H., Sun M., Sun Y., Ni R., Sun J., Huang D.: Noninvasive *in vivo* imaging and monitoring of 3D-printed polycaprolactone scaffolds labeled with an NIR region II fluorescent dye. ACS Applied Bio Materials, **4**, 3189–3202 (2021). https://doi.org/10.1021/acsabm.0c01587

[11] Yang C., Gao X., Younis M. R., Blum N. T., Lei S., Zhang D., Luo Y., Huang P., Lin J.: Non-invasive monitoring of *in vivo* bone regeneration based on alkaline phosphatase-responsive scaffolds. Chemical Engineering Journal, **408**, 127959 (2021). https://doi.org/10.1016/j.cej.2020.127959

[12] Li X., Zou Q., Wei J., Li W.: The degradation regulation of 3D printed scaffolds for promotion of osteogenesis and *in vivo* tracking. Composites Part B: Engineering, **222**, 109084 (2021). https://doi.org/10.1016/j.compositesb.2021.109084

[13] Tai C-L., Hong W-L., Kuo Y-T., Chang C. Y., Niu M. C., Ochathevar M. K. P., Hsu C. L., Horng S. F., Chao Y. C.: Ultrastable, deformable, and stretchable luminescent organic-inorganic perovskite nanocrystal-polymer composites for 3D printing and white light-emitting diodes. ACS Applied Materials and Interfaces, **11**, 30176–30184 (2019). https://doi.org/10.1021/acsami.9b06248

[14] Wang K., Luo Y., Huang S., Yang H., Liu B., Wang M.: Highly fluorescent polycaprolactones decorated with di(thiophene-2-yl)-diketopyrrolopyrrole: A covalent strategy of tuning fluorescence properties in solid states. Journal of Polymer Science Part A: Polymer Chemistry, **53**, 1032–1042 (2015). https://doi.org/10.1002/pola.27531

[15] Cho H. K., Lone S., Kim D. D., Choi J. H., Choi S. W., Cho J. H., Kim J. H., Cheong I. W.: Synthesis and characterization of fluorescein isothiocyanate (FITC)-labeled PEO–PCL–PEO triblock copolymers for topical delivery. Polymer, **50**, 2357–2364 (2009). https://doi.org/10.1016/j.polymer.2009.03.032

[16] Zhu Y-H., Wang J-L., Zhang H-B., Khan M. I., Du X-J., Wang J.: Incorporation of a rhodamine B conjugated polymer for nanoparticle trafficking both *in vitro* and *in vivo*. Biomaterials Science, **7**, 1933–1939 (2019). https://doi.org/10.1039/c9bm00032a

[17] Zhang D. H., Jia D. M., Chen S. F.: Synthesis and characterization of low viscosity aromatic hyperbranched poly(trimellitic anhydride ethylene glycol) ester epoxy resin. Macromolecular Chemistry and Physics, **210**, 1159–1166 (2009). https://doi.org/10.1002/macp.200900230

[18] Wang Y., Chen S., Chen X., Lu Y., Miao M., Zhang D.: Controllability of epoxy equivalent weight and performance of hyperbranched epoxy resins. Composites Part B: Engineering, **160**, 615–625 (2019). https://doi.org/10.1016/j.compositesb.2018.12.103

[19] Zhang K., Cheng F., Lin Y., Zhou M., Zhu P-X.: Effect of hyperbranched poly(trimellitic glyceride) with different molecular weight on starch plasticization and compatibility with polyester. Carbohydrate Polymers, **195**, 107–113 (2018). https://doi.org/10.1016/j.carbpol.2018.04.080

[20] Huang W., Yan H., Niu S., Du Y., Yuan L.: Unprecedented strong blue photoluminescence from hyperbranched polycarbonate: From its fluorescence mechanism to applications. Journal of Polymer Science Part A: Polymer Chemistry, **55**, 3690–3696 (2017). https://doi.org/10.1002/pola.28754

[21] Yuan L., Yan H., Bai L., Bai T., Zhao Y., Wang L., Feng Y.: Unprecedented multicolor photoluminescence from hyperbranched poly(amino ester)s. Macromolecular Rapid Communications, **40**, e1800658 (2019). https://doi.org/10.1002/marc.201800658

[22] Lee K. W., Chung J. W., Kwak S-Y.: Flexible poly(vinyl chloride) nanocomposites reinforced with hyperbranched polyglycerol-functionalized graphene oxide for enhanced gas barrier performance. ACS Applied Materials and Interfaces, **9**, 33149–33158 (2017). https://doi.org/10.1021/acsami.7b10257

[23] Zhu Q., Qiu F., Zhu B., Zhu X.: Hyperbranched polymers for bioimaging. RSC Advances, **3**, 2071–2083 (2013). https://doi.org/10.1039/c2ra22210h

[24] Sun C., Jiang X., Li B., Li S., Kong X. Z.: Fluorescence behavior and mechanisms of poly(ethylene glycol) and their applications in Fe^{3+} and Cr^{6+} detections, data encryption, and cell imaging. ACS Sustainable Chemistry and Engineering, **9**, 5166–5178 (2021). https://doi.org/10.1021/acssuschemeng.1c00250

[25] Gadomska-Gajadhur A., Bandzerewicz A., Wrzecionek M., Ruśkowski P.: Biobased poly(glycerol citrate) synthesis optimization *via* design of experiments. Polymers for Advanced Technologies, **32**, 3982–3994 (2021). https://doi.org/10.1002/pat.5498

[26] Adeli M., Rasoulian B., Saadatmehr F., Zabihi F.: Hyperbranched poly(citric acid) and its application as anticancer drug delivery system. Journal of Applied Polymer Science, **129**, 3665–3671 (2013). https://doi.org/10.1002/app.39028

[27] Yang M-L., Wu Y-X., Liu Y., Qiu J-J., Liu C-M.: A novel bio-based AB_2 monomer for preparing hyperbranched polyamides derived from levulinic acid and furfurylamine. Polymer Chemistry, **10**, 6217–6226 (2019). https://doi.org/10.1039/c9py01253b

[28] Jiang S., Muller E., Jerôme F., Pera-Titus M., de Oliveira Vigier K.: Conversion of furfural to tetrahydrofuran-derived secondary amines under mild conditions. Green Chemistry, **22**, 1832–1836 (2020). https://doi.org/10.1039/d0gc00119h

[29] Hazarika D., Karak N.: Waterborne sustainable tough hyperbranched aliphatic polyester thermosets. ACS Sustainable Chemistry and Engineering, **3**, 2458–2468 (2015). https://doi.org/10.1021/acssuschemeng.5b00494

[30] Ghosh T., Karak N.: Biobased multifunctional macroglycol containing smart thermoplastic hyperbranched polyurethane elastomer with intrinsic self-healing attribute. ACS Sustainable Chemistry and Engineering, **6**, 4370–4381 (2018). https://doi.org/10.1021/acssuschemeng.8b00001

[31] Zhang K., Cheng X., Cheng F., Lin Y., Zhou M., Zhu P.: Poly(citrate glyceride): A hyperbranched polyester for starch plasticization. Polymer International, **67**, 399–404 (2018). https://doi.org/10.1002/pi.5520

[32] Wu J., Chen J., Wang J., Liao X., Xie M., Sun R.: Synthesis and conductivity of hyperbranched poly(triazolium)s with various end-capping groups. Polymer Chemistry, **7**, 633–642 (2016). https://doi.org/10.1039/C5PY01735A

[33] Aerts J.: Prediction of intrinsic viscosities of dendritic, hyperbranched and branched polymers. Computational and Theoretical Polymer Science, **8**, 49–54 (1998). https://doi.org/10.1016/S1089-3156(98)00013-0

[34] Xing A., Miao X., Liu T., Yang H., Meng Y., Li X.: An intrinsic white-light-emitting hyperbranched polyimide: Synthesis, structure–property and its application as a 'turn-off' sensor for iron(III) ions. Journal of Materials Chemistry C, **7**, 14320–14333 (2019). https://doi.org/10.1039/c9tc04102h

[35] Du Y., Yan H., Huang W., Chai F., Niu S.: Unanticipated strong blue photoluminescence from fully biobased aliphatic hyperbranched polyesters. ACS Sustainable Chemistry and Engineering, **5**, 6139–6147 (2017). https://doi.org/10.1021/acssuschemeng.7b01019

[36] Du Y., Bai T., Yan H., Zhao Y., Feng W., Li W.: A simple and convenient route to synthesize novel hyperbranched poly(amine ester) with multicolored fluorescence. Polymer, **185**, 121771 (2019). https://doi.org/10.1016/j.polymer.2019.121771

[37] Sun C., Jiang X., Li B., Li S., Kong X. Z.: Fluorescence behavior and mechanisms of poly(ethylene glycol) and their applications in Fe^{3+} and Cr^{6+} detections, data encryption, and cell imaging. ACS Sustainable Chemistry and Engineering, **9**, 5166–5178 (2021). https://doi.org/10.1021/acssuschemeng.1c00250

[38] Yuan Z. W., Zhang Y.: Nonconventional macromolecular luminogens with aggregation-induced emission characteristics. Journal of Polymer Science Part A: Polymer Chemistry, **55**, 560–574 (2017). https://doi.org/10.1002/pola.28420

[39] Liu J., Chen Z., Hu C., Yang W., Wang J., Xu W., Wang Y., Ruan C., Luo Y.: Fluorescence visualization directly monitors microphase separation behavior of shape memory polyurethanes. Applied Materials Today, **23**, 100986 (2021). https://doi.org/10.1016/j.apmt.2021.100986

[40] Han T., Gui C., Lam J. W. Y., Jiang M., Xie N., Kwok R. T. K., Tang B. Z.: High-contrast visualization and differentiation of microphase separation in polymer blends by fluorescent AIE probes. Macromolecules, **50**, 5807–5815 (2017). https://doi.org/10.1021/acs.macromol.7b00973

[41] Lin Y., Zhang K-Y., Dong Z-M., Dong L-S., Li Y-S.: Study of hydrogen-bonded blend of polylactide with biodegradable hyperbranched poly(ester amide). Macromolecules, **40**, 6257–6267 (2007). https://doi.org/10.1021/ma070989a

[42] Zhang Y., Zhuo P., Yin H., Fan Y., Zhang J., Liu X., Chen Z.: Solid-state fluorescent carbon dots with aggregation-induced yellow emission for white light-emitting diodes with high luminous efficiencies. ACS Applied Materials and Interfaces, **11**, 24395–24403 (2019). https://doi.org/10.1021/acsami.9b04600

[43] Adsetts J. R., Hoesterey S., Gao C., Love D. A., Ding Z.: Electrochemiluminescence and photoluminescence of carbon quantum dots controlled by aggregation-induced emission, aggregation-caused quenching, and interfacial reactions. Langmuir, **36**, 14432–14442 (2020). https://doi.org/10.1021/acs.langmuir.0c02886

[44] Li B., Xu C., Liu L., Yu J., Fan Y.: Facile and sustainable etherification of ethyl cellulose towards excellent UV blocking and fluorescence properties. Green Chemistry, **23**, 479–489 (2021). https://doi.org/10.1039/d0gc02919j

[45] Madbouly S. A.: Nano/micro-scale morphologies of semi-interpenetrating poly(ε–caprolactone)/tung oil polymer networks: Isothermal and non–isothermal crystallization kinetics. Polymer Testing, **89**, 106586 (2020). https://doi.org/10.1016/j.polymertesting.2020.106586

[46] Nile R., Rajput H., Sims C., Jin K.: Sensing the melting transition of semicrystalline polymers *via* a novel fluorescence technique. Polymer, **230**, 124070 (2021). https://doi.org/10.1016/j.polymer.2021.124070